
**Showcasing work from a consortium of analysts, electrochemists and material scientists from KIST, UTS and the Gyeongsang National University.**

**Title: High capacity cathode materials for Li–S batteries**

This work introduces a stable sulfur cathode for high energy Li/S batteries. A sulfur–activated carbon composite is prepared by encapsulating sulfur into the activated carbon micropores by a solution-based processing technique. The elemental sulfur exists in a highly dispersed state inside the activated carbon micropores.

**As featured in:**

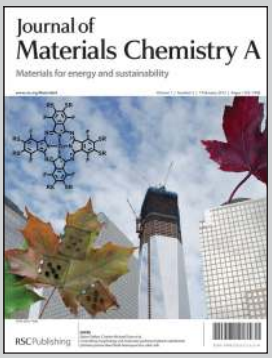


See H. S. Ryu *et al.*, *J. Mater. Chem. A*, 2013, **1**, 1573.

RSC Publishing

www.rsc.org/MaterialsA

Registered Charity Number 207890

Journal of Materials Chemistry A

RSC Publishing

PAPER

# High capacity cathode materials for Li–S batteries†

Cite this: *J. Mater. Chem. A*, 2013, **1**, 1573

Ho Suk Ryu,[a] Jin Woo Park,[a] Jinsoo Park,[a] Jae-Pyeung Ahn,[b] Ki-Won Kim,[a] Jou-Hyeon Ahn,*[c] Tae-Hyeon Nam,[a] Guoxiu Wang[ad] and Hyo-Jun Ahn*[a]

Received 24th August 2012
Accepted 8th November 2012

DOI: 10.1039/c2ta00056c

www.rsc.org/MaterialsA

To enhance the stability of sulfur cathode for a high energy lithium–sulfur battery, sulfur–activated carbon (S–AC) composite was prepared by encapsulating sulfur into micropores of activated carbon using a solution-based processing technique. In the analysis using the prepared specimen of S–AC composite by the focused ion beam (FIB) technique, the elemental sulfur exists in a highly dispersed state inside the micropores of activated carbon, which has a large surface area and a narrow pore distribution. The S–AC composite was characterized through X-ray powder diffraction (XRD), transmission electron microscopy (TEM), Brunauer–Emmett–Teller (BET) method, selected area electron diffraction (SAED), energy dispersive X-ray spectrometry (EDX), Fourier transform infrared spectroscopy (FT-IR), thermogravimetry analysis (TGA), and field emission scanning electron microscopy (FESEM). A lithium–sulfur cell using the S–AC composite has a high first discharge capacity over 800 mA h $g^{-1}$ S even at a high current density such as 2*C* (3200 mA $g^{-1}$ S) and has good cycleability around 500 mA h $g^{-1}$ S discharge capacity at the 50$^{th}$ cycle at the same current density.



## Introduction

The development of high energy density rechargeable batteries becomes more and more important for clean and efficient energy storage and conversion technologies, such as in modern communication devices, electric vehicles (EVs), and electrical storage from wind and solar power. However, batteries for large-scale power applications require a much higher energy density and low cost. In the pursuit of energy materials for lighter, cheaper and non-toxic batteries with high specific energy, lithium–sulfur (Li–S) batteries have gained great attraction. The Li–S battery works on the basis of redox reactions between a lithium metal anode and a sulfur cathode. The combination of lithium metal with a theoretical specific capacity of 3830 mA h $g^{-1}$ as the anode and elemental sulfur (S) with a theoretical specific capacity of 1675 mA h $g^{-1}$ as the cathode in a battery can generate a high theoretical specific energy of 2600 W h $kg^{-1}$.[1–3]

Recently, many results have been reported on the improvement of specific capacity and cycling performance of the Li–S batteries from preparation of a sulfur–carbon composite by reduction of the sulfur particle size and the distribution of sulfur into pores of carbon by thermal processing technology.[4–16]

Among the many results, Li–S battery using S-mesoporous carbon composites[4,5] had high discharge capacity and good cycle life by adsorption of reaction products in mesopores. To prepare mesoporous carbon such as CMK, silica template SBA-15 was firstly prepared with controlled morphology. A nanocasting method was used to fabricate CMK-3 from SBA-15 as a hard template which is also prepared by a complicated method with various processes such as mixing, pre-heating, addition and heating with high pressure. However, the reported processes using mesoporous carbon involved a series of complicated physical and chemical methods with the prolonged preparation time and the using of expensive materials, which is likely to offset the advantage of low-cost sulfur battery.

However, activated carbon (AC) among various carbons is a commercialized and inexpensive material, originated from the carbonization of various source materials like nutshells, peat, wood, coir, lignite, coal and petroleum pitch. AC has been historically used for removal of odor, color pigments and various catalytic functions. It is well known that the activated carbon (AC) has micropores, various pore distribution and a high specific surface area (SSA). Applications of activated carbon have increased significantly in the recent years with the advancement of the activation process capability and it is widely used in various fields such as adsorption of heavy metals, liquid or vapour purification, catalytic functions in fuel cells, anode materials, *etc.*[17–21] Recently, the AC has been applied to lithium batteries.[22,23]

[a]*School of Materials Science and Engineering, RIGET, PRC for Nano-morphic Biological Energy Conversion and Storage, Gyeongsang National University, Jinju-daero 501, Jinju, Gyeongnam 660-701, Republic of Korea. E-mail: fangy@gnu.ac.kr; ahj@gnu.ac.kr; Fax: +82-55-772-1666; Tel: +82-55-762-8657*

[b]*Advanced Analysis Center, Research Planning & Coordination Division, PRC for Nano-morphic Biological Energy Conversion and Storage, KIST, Hwarangno 14-gil 5, Seongbuk-gu, Seoul, 136-791, Republic of Korea. E-mail: jpahn@kist.re.kr; Tel: +82-02-958-5536*

[c]*Department of Chemical and Biological Engineering, Gyeongsang National University, Jinju-daero 501, Jinju, Gyeongnam 660-701, Republic of Korea. E-mail: jhahn@gnu.ac.kr; Fax: +82-55-772-1666; Tel: +82-55-772-2651*

[d]*School of Chemistry and Forensic Science, University of Technology Sydney, City Campus, Broadway, Sydney, NSW 2007, Australia. E-mail: Guoxiu.Wang@uts.edu.au*

† Electronic supplementary information (ESI) available. See DOI: 10.1039/c2ta00056c

Chen *et al.*[22] prepared the sulfur–activated carbon composites (S–AC composites) by a mixing and heating process of two steps: at 150 °C and 300 °C. They reported that the Li/S–AC composite battery had a high discharge capacity of 1180.8 mA h $g^{-1}$ at first discharge and a good cycle life at 720.4 mA h $g^{-1}$ after 60 cycles in the low current density (100 mA $g^{-1}$ S). However, the authors did not discuss on the location, the distribution and the state of sulfur inside activated carbon particles.

In this study, we prepared an S–AC composite using an AC such as BP-20 through a simple solution-based processing technique. The S–AC composite was investigated for the location, the distribution and the state of sulfur in the S–AC composite by analyzing accurately through FT-IR, SAED, electron-energy loss spectroscopy (EELS), TEM, and high resolution transmission electron microscopy (HRTEM) combined with the FIB technique. The electrochemical properties of the S–AC composite were investigated with the high current density.

## Experimental

### Preparation of the composite

An activated carbon (Kuraray Chemical) powder has a pore volume of 0.7932 $cm^3$ $g^{-1}$, an SSA of 1696 $m^2$ $g^{-1}$ and an average pore diameter of 1.87 nm by result of BET analysis. Sulfur (Aldrich Co.) and AC were pre-treated at 60 °C and 1000 °C, respectively. A weight ratio of 10 : 3 of sulfur and AC powder was used to prepare S–AC composites. As calculated below, the 1.6419 g sulfur can fully fill the pore volume of 1 g AC. In other words, the maximum sulfur content is 62.15 wt% of the S–AC composite.

$$\text{Sulfur content (g)} = \text{sulfur density (g cm}^{-3}) \times \text{pore volume (cm}^3)$$

$$\text{Sulfur weight ratio in the S–AC composite (\%)} = \text{sulfur content/S–AC composite} \times 100$$

$$\text{S–AC composite} = \text{sulfur content} + \text{carbon content}$$

A solution-based processing technique was employed for the preparation of S–AC composite as shown in Fig. 1. In the first step, sulfur powder was dissolved in dimethyl sulfoxide (DMSO) by heating to 90 °C. The AC powder was added to the solution and dispersed by magnetic stirring for 3 h. Afterward the mixture was cooled to room temperature while being stirred. During cooling, the dissolved sulfur was recrystallized in the activated carbon and formed a sulfur–carbon composite in the solution. After that, the composite powder was separated by a centrifuge and washed with ethanol to remove the residual DMSO several times, and then dried in a vacuum at room temperature to evaporate ethanol. The composite showed 54.27 wt% sulfur from the result of TGA (Q50, TA instrument). It is lower than the added sulfur powder content 76.92 wt% and also the theoretical amount (62.15 wt%). Apparently, some amount of sulfur (22.65 wt%) did not recrystallize in the composite powder after being dissolved in DMSO solvent and was washed away by ethanol at the dissolving state.

### Characterization of materials

The morphology of AC and the S–AC composite was observed using a field emission scanning electron microscope (FESEM, Hitachi S-4200) and a scanning transmission electron microscope (STEM). The pore volume, SSA and average pore diameter were calculated using the BET method. In order to confirm the location, the distribution and the state of sulfur in the S–AC composite, it is necessary to observe sulfur in the S–AC composite particle.

Therefore, a thin specimen for the inside of the S–AC composite particle was prepared by the FIB (FEI Nova 600 Dual Beam FIB) technique. The S–AC composite particle was etched except for a selected area using $Ga^+$ liquid-metal ion sources (LMIS). After destructive sputtering on the particle a thin specimen piece was lifted out and mounted on a TEM and the HRTEM (FEI Titan 80-300) specimen support. All the processes were carried out by an *in situ* lift-out (ISLO) method. The specimen was fixed by depositing platinum. The location, the distribution and the state of sulfur in the S–AC composite were observed using the scanning transmission electron microscope (STEM), the TEM and EDX with S–AC composite specimen by the FIB technique. For the state of sulfur in the S–AC composite, the FTIR data were recorded using KBr pellets on a VERTEX 80v (Bruker Optics) FT-IR spectrophotometer.

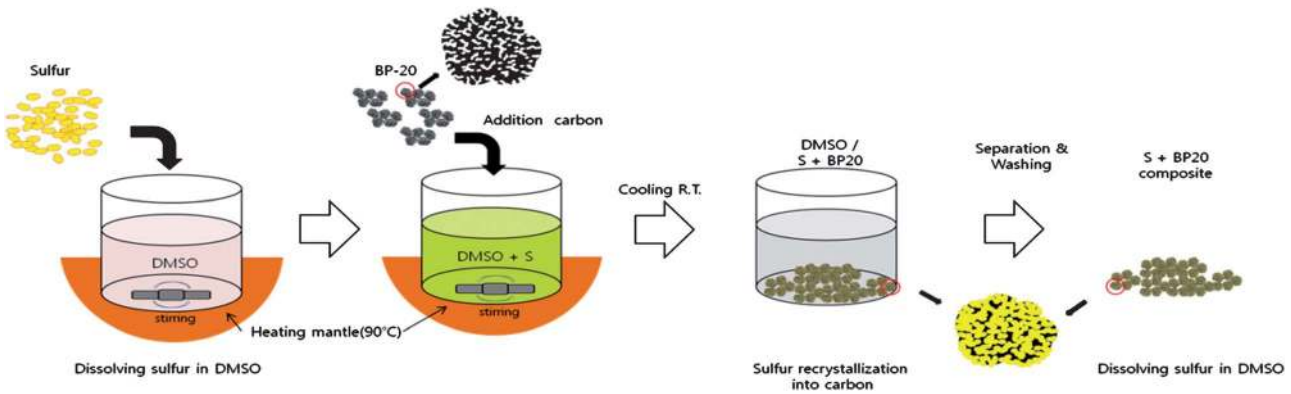


**Fig. 1** Schematic of the solution processing for the preparation of S–AC composites.

 

### Electrochemical test

For the preparation of an S–AC electrode, the S–AC composite, poly(vinylidene fluoride) (PVdF, Aldrich Co.) as a binder and acetylene black (Aldrich Co.) as a conducting material were homogeneously mixed in *N*-methyl-2-pyrrolidinone solvent using planetary ball milling. An S–AC electrode was composed of 60 wt% S–AC composite, 20 wt% acetylene black (AB), and 20 wt% PVdF. The mixed slurry was coated on an aluminium foil and dried under vacuum at 60 °C for 24 h to remove solvent and moisture. The S–AC electrodes were punched into circular disks with a diameter of 10 mm. A Swagelok type Li/S–AC cell was fabricated by stacking lithium metal anode, Celgard1 2400 separator film with liquid electrolyte and S–AC cathode. The liquid electrolyte for Li/S–AC battery was prepared by mixing 1 M lithium bis(trifluoromethane sulfonyl)imide ($LiN(SO_2CF_3)_2$, Aldrich Co.) in 1,2-dimethoxyethane (DME, Aldrich Co.) and 1,3-dioxolane (DOXL, Aldrich). The cell assembly was performed under an argon atmosphere in a glove box. The charge/discharge cycling tests were performed on a WonA tech WBCS 3000L battery test system in galvanostatic mode with cut-off voltages of 1.5 V and 2.8 V at room temperature. The scanning rate for the CV measurement was 0.1 mV $s^{-1}$.

## Results and discussion

The morphologies of AC and the S–AC composite were observed by FESEM and their surface was measured by BET. In the FESEM image of Fig. 2, both the particles show a broad size distribution from several tens of micron size to submicron. In the SEM image, the S–AC composite nearly is similar in the surface morphology and size to AC. However, the specific surface areas (SSA) of the S–AC composite decreased to 0.0033 $m^2$ $g^{-1}$ from 1696 $m^2$ $g^{-1}$ of AC. It is proved that sulfur was successfully embedded into the pores of the AC and the surface of the carbon was clad with sulfur.

Fig. 3 shows TEM and HRTEM images of an AC particle ((a) and (b)) and an S–AC composite ((c) and (d)). Fig. 3(b) shows the typical amorphous carbon pattern. The pores probably exist between typical amorphous carbon patterns. In the TEM image of the S–AC composite particle in Fig. 3(c), there is no morphological difference from Fig. 3(a). The amorphous carbon structure of AC was not changed after the incorporation of sulfur. For a clear view of the sulfur state in AC, sulfur on the surface of the S–AC composite was removed by heating at 300 °C for 10 min. After heat treatment, the sulfur content of the composite decreased to 45.59 from 54.27 wt%. It means that sulfur filled 73.35% of the pore volume inside AC.

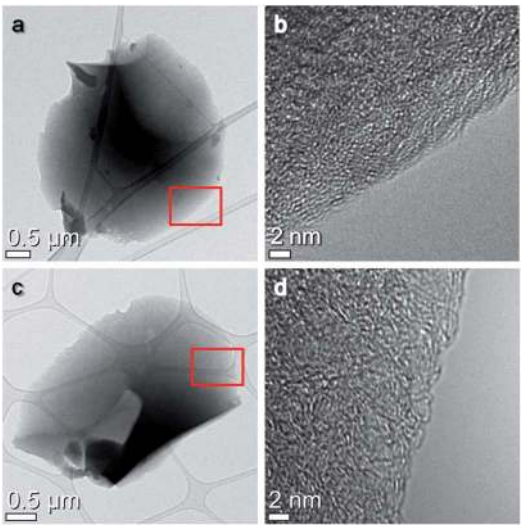


**Fig. 3** TEM and HRTEM images; AC ((a) and (b)) and S–AC composite ((c) and (d)) with heat treatment (300 °C for 10 min).

Fig. 4 presents a High-Angle Annular Dark-Field (HAADF) STEM image of the S–AC composite particle. In this image, the different contrast is related to the different thickness of the particle. A bright region (O1) and a dark region (O2) are referred to thick and thin areas, respectively. From the sulfur content with carbon thickness, the sulfur penetration depth into pores of the AC was measured by EDX. In the thick and the thin part, the ratio of sulfur and carbon was almost similar. From this analysis, it was proved that the homogeneity of sulfur in the S–AC composite is achieved even on the inside of the particle. Therefore, sulfur should penetrate along arbitrarily misaligned channels of nanopores.

From the results of BET and STEM, sulfur in the S–AC composite was infiltrated deep within the open pores on the surface of the AC particle. However, the infiltration depth, contents and state of sulfur in the overall S–AC composite were still unknown. To our knowledge, mesoporous carbon powder

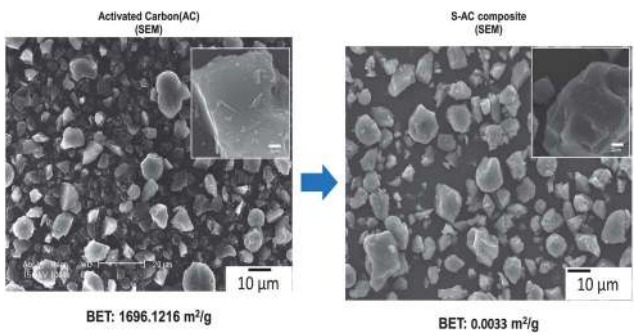


**Fig. 2** SEM image and surface area of AC and S–AC composite.

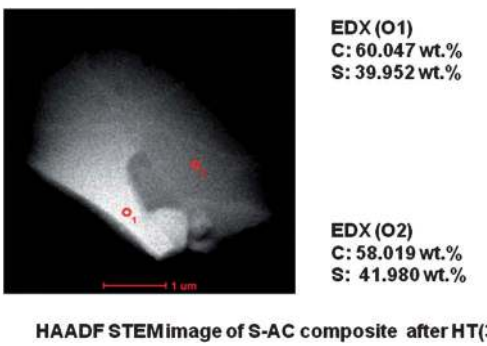


**Fig. 4** STEM and EDX of S–AC composite.

with average 3 nm pore diameter provides direct evidence for the existence of sulfur in the structure by TEM observation. Nazar *et al.*[5] reported filling the carbon channels with sulfur was corroborated by the TEM image and EDX mapping of sulfur and carbon clearly demonstrated that sulfur was homogeneously distributed in the framework of the mesoporous carbon, with no significant fraction on the external surface. J. Wang *et al.*[4] reported that sulfur also exists inside the mesoporous carbon in the amorphous state by SAED analysis of sulfur–mesoporous carbon powder, but the sample was thick for observation of the inside of mesoporous carbon powder with several tens of nanometers. Herein, a study on filtration depth of sulfur, its content, distribution and state at the inner S–AC composite particle was carried out using EDX, SAED, HRTEM and electron energy loss spectroscopy (EELS) with a TEM specimen of the S–AC composite particle by the FIB technique. Fig. 5 shows a scheme of the specimen by FIB and a TEM image of the specimen which has a thickness of a few nanometers. A composite particle was chopped like slices by high energy $Ga^+$ liquid-metal ion sources. To the best of our knowledge, this is the first time to investigate the state and the content of sulfur in AC by the FIB technique.

In the HRTEM image of the S–AC specimen in Fig. 6(a), the pattern of S–AC is similar to the amorphous structure of the AC. The selected area electron diffraction (SAED) pattern in Fig. 6(b) shows no characteristic rings but a blurred amorphous phase. The microstructure of the AC is maintained in spite of the existence of sulfur inside the AC structure. In the SAED result of Fig. 6(b), the AC structure was unchanged throughout the synthetic procedure as an amorphous state and sulfur also exits inside the AC structure in the amorphous state. Our result is in accordance with DSC and XRD results after heat treatment of the S–AC composite for 10 min at 300 °C. Except for the AC peaks, no other peaks are found in DSC and XRD results (ESI Fig. X2 and X3†). It is confirmed that the remaining sulfur inside the AC has an amorphous structure from the results of HRTEM, SAED, DSC and XRD.

Fig. 7 presents a STEM image and its EDX result in different parts of the S–AC composite specimen. The sulfur content is slightly altered between 20 and 30 wt% in the four parts. It is indicated that sulfur is dispersed in the AC from outside to inside. The sulfur content is lower than in the TGA result because of the loss of sulfur by $Ga^+$ liquid-metal ion sources of FIB.

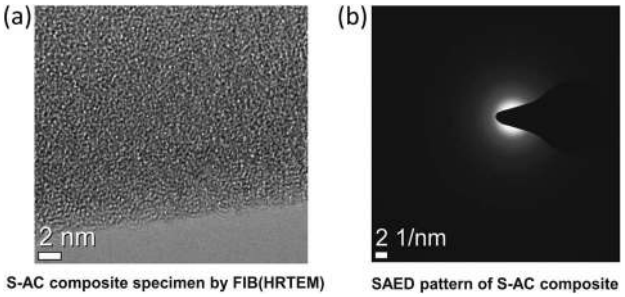


**Fig. 6** HRTEM image and SAED pattern of S–AC composite specimen by FIB.

Fig. 8 shows FTIR spectra of sulfur powder, the AC powder and the S–AC composite. Sulfur shows vibrations at 1636, 2857, 2919 and 3433 $cm^{-1}$ and the AC powder has vibrations below 700 $cm^{-1}$. It is found that the spectra of the S–AC composite sample had similar vibrations with sulfur, indicating no chemical reaction happened between sulfur and the AC under this synthesis method. From this result, sulfur on the inside of the AC has S–S bonding but does not have the S–C bond. This result is proved by the EELS result (ESI, Fig. X5†) of the S–AC composite specimen. However, the peaks of sulfur are not observed in the XRD and DSC results of the S–AC composite. It is probably because the size of the covalent sulfur atom is close to 1 Å and the S–S bonding length is 1.887 Å in S–S($S_2$); even though the status of sulfur is crystalline as S–S($S_2$) inside of the AC, the confined sulfur is close to amorphous.

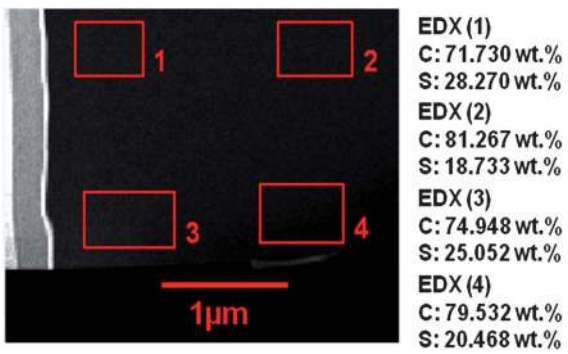


**Fig. 7** STEM image and EDX in various parts of S–AC composite specimen by FIB with heat treatment (300 °C for 10 min).

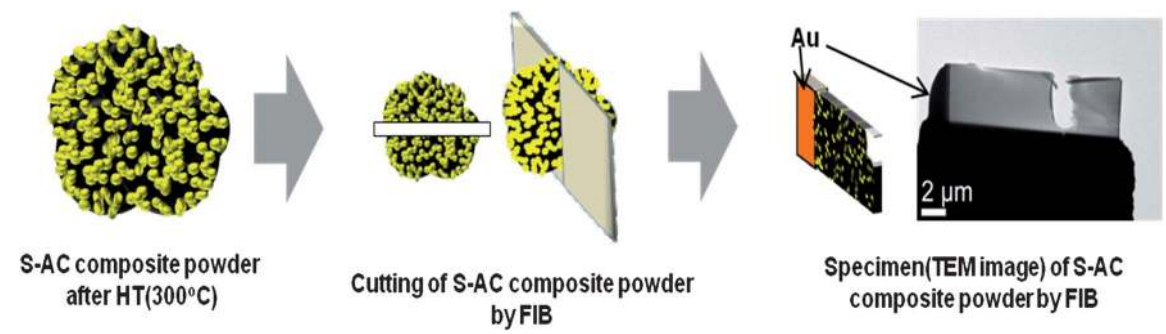


**Fig. 5** Schematic of composite specimen by FIB and TEM image of the specimen.

 

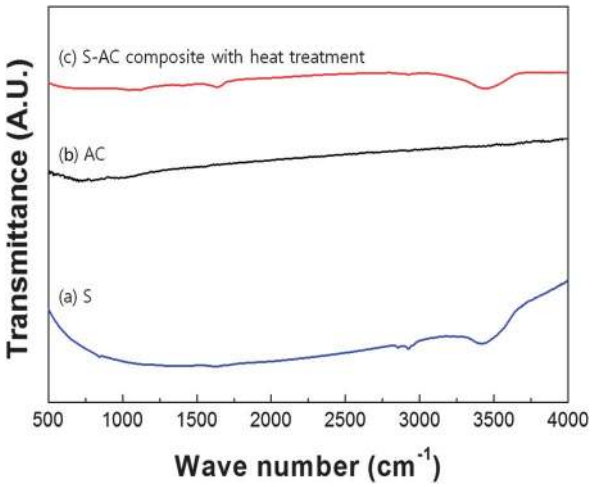


**Fig. 8** FTIR spectra of the powders: (a) S, (b) AC and (c) S–AC composite with heat treatment (300 °C for 10 min).

Fig. 9 shows electrochemical properties of Li battery using the S–AC composite as the cathode active material. Fig. 9(a) shows the cyclic voltammetry (CV) curves of the S–AC composite electrode in the voltage window of 1.5–2.8 V. As the AC is electrochemically inert in this voltage range, the redox peaks can only be ascribed to the redox reactions associated with sulfur and lithium ions. In the first cycle, the CV curve has two cathodic peaks at 2.35 V and 2.08 V, which can be assigned to the reduction processes of sulfur. The first cathodic peak at around 2.35 V corresponds to the reduction of elemental sulfur to polysulfide. As the reduction proceeds, lithium polysulfides are reduced to lithium sulfides, which should be responsible for the second cathodic peak at 2.08 V. The anodic peak of 2.27 V and 2.42 V represents a reversible process from lithium sulfides to elemental sulfur. The reactions of discharge are in accordance with the typical sulfur of chemical formulae as follows.[1,24]

$$xLi^+ + S_8 + e^- \rightarrow Li_2S_x \text{ (2.4–2.1 V)} \quad (1)$$

$$Li_2S_x + Li^+ + e^- \rightarrow Li_2S_2 \text{ or } Li_2S \text{ (2.1–1.5 V)} \quad (2)$$

From the second cycle, the intensities of the two reduction peaks at 2.35 V and 2.08 V decrease and the reduction peaks shift slightly to a lower potential (2.32 V and 2.05 V). From the oxidation peaks of the second cycle, the peaks shift to a higher potential slightly. However, the intensity of 2.42 V decreases, while the intensity of 2.30 V increases in the oxidation peak of the second cycle. After the second cycle, the peak potential and intensity are kept unchanged in the 3rd cycle.

Fig. 9(b) shows the first charge–discharge curves of the S–AC composite electrodes at different current densities. Two discharge plateaus can be easily distinguished in the voltage ranges of 2.4–2.1 V and 2.1–1.5 V, respectively. These two discharge plateaus match very well with the two cathodic peaks in the CV curves as shown in Fig. 9(a). The S–AC composite delivers the highest specific discharge capacity of 1364.3, 1137.8 and 801.3 mA h $g^{-1}$ at 400 mA $g^{-1}$ ($\fallingdotseq$ 0.25*C*), 1600 mA $g^{-1}$ ($\fallingdotseq$ 1*C*) and 3200 mA $g^{-1}$ ($\fallingdotseq$ 2*C*) in the first cycle, respectively.

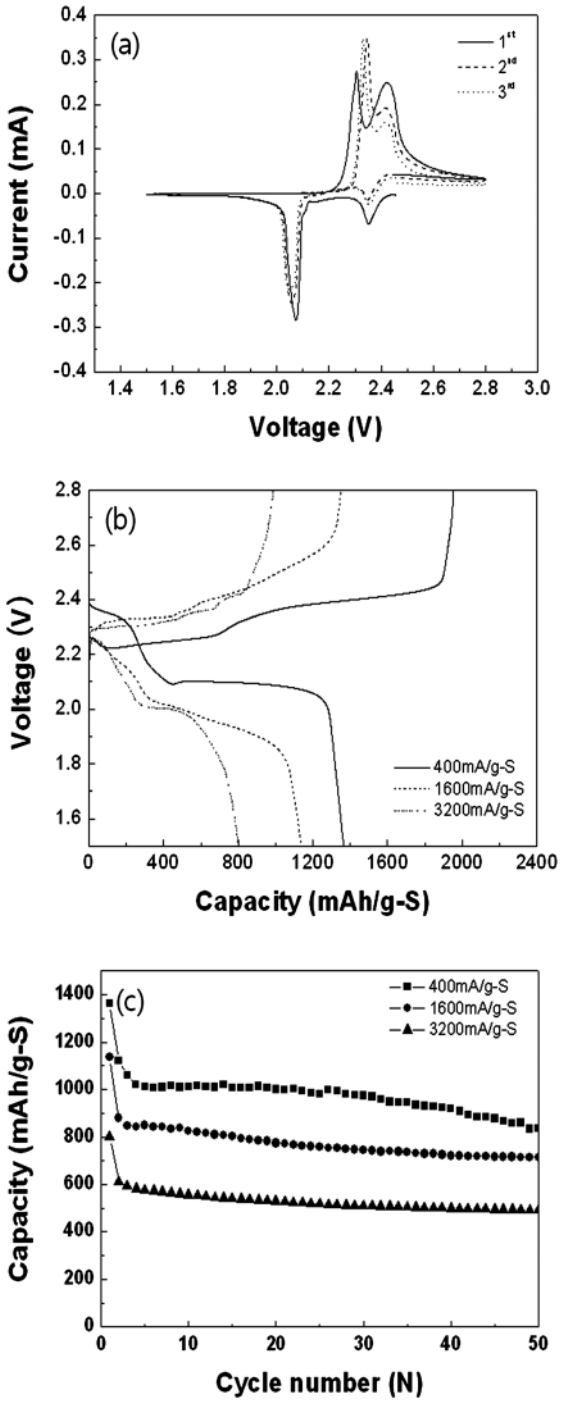


**Fig. 9** Electrochemical properties of Li battery using S–AC composite cathode; (a) CV (the scanning rate is 0.1 mV $s^{-1}$) and (b) charge–discharge curves and (c) cycle life with current density.

Fig. 9(c) shows the cycling performance of the S–AC composite electrodes at different *C*-rates to be 0.25*C*, 1*C* and 2*C*, respectively. The S–AC composite cathodes deliver the highest specific discharge capacity in the first cycle and then decline for a few cycles due to easier dissolution of sulfur on the carbon surface into electrolyte. After the 50th cycle, the discharge capacity of 835, 714 and 493 mA h $g^{-1}$ remained at 0.25*C*, 1*C* and 2*C*, respectively. It means that sulfur in the inner part of AC

was well retained and is difficult to be dissolved into the electrolyte.

He *et al.*[25] reported that the sulfur composite electrodes expanded when discharging and shrank when charging. The thickness change of the electrode was measured to be about 22%. For improving the cycle life, it is necessary to keep sulfur in carbon pores and control its content in the S–AC composite. Because the volume of the active materials was increased by the formation of lithium sulfide during discharging by reaction with lithium as in eqn (1), the loss of the active materials can occur. By the calculation of the mass of sulfur accommodated in the pore space from the pore volume of the AC, the suitable sulfur content in this S–AC composite is 40.78 wt%.

Consequently, the high utilization of active materials and a long cycle life can be obtained through the minimum loss of active material and the homogeneous distribution of sulfur into AC pores by solution-based processing in this study.

## Conclusions

An activated carbon with a high specific surface area of 1696 $m^2$ $g^{-1}$ is used to prepare an S–AC composite as a cathode active material for Li–S batteries by a novel solution-based processing technique. Applying the FIB technique, the state and the content of sulfur inside carbon micropores are firstly investigated. It is found that sulfur exists as S–S bonding and is uniformly distributed in the pores of the AC particle from outside to inside. Li–S batteries with the S–AC composite cathode show good electrochemical properties and high discharge capacities over 800 mA h $g^{-1}$ at 2*C* and about 500 mA h $g^{-1}$ after 50 cycles are obtained.

## Acknowledgements

This research was supported by 'Pioneer Research Center for Nano-morphic Biological Energy Conversion and Storage' and 'WCU Center for Next Generation Battery' through the Korea Science and Engineering Foundation (KOSEF) funded by the Ministry of Education, Science and Technology.

## Notes and references

1 R. D. Rauh, K. M. Abraham, G. F. Pearson, J. K. Surprenant and S. B. Brummer, *J. Electrochem. Soc.*, 1979, **126**, 523.
2 J. Shim, K. A. Striebel and E. J. Cairns, *J. Electrochem. Soc.*, 2002, **149**, A1321.
3 D. Peramunage and S. Licht, *Science*, 1993, **261**, 1029.
4 J. Wang, S. Y. Chew, Z. W. Zhao, S. Ashraf, D. Wexler, J. Chen, S. H. Ng, S. L. Chou and H. K. Liu, *Carbon*, 2008, **46**, 229.
5 X. Ji, K. T. Lee and L. F. Nazar, *Nat. Mater.*, 2009, **8**, 500.
6 B. Zhang, C. Lai, Z. Zhou and X. P. Gao, *Electrochim. Acta*, 2009, **54**, 3708.
7 L. Yuan, H. Yuan, X. Qiu, L. Chen and W. Zhu, *J. Power Sources*, 2009, **189**, 1141.
8 J.-J. Chen, X. Jia, Q.-J. She, C. Wang, Q. Zhang, M.-S. Zheng and Q.-F. Dong, *Electrochim. Acta*, 2010, **55**, 8062.
9 J.-Z. Wang, L. Lu, M. Choucair, J. A. Stride, X. Xu and H.-K. Liu, *J. Power Sources*, 2011, **196**, 7030.
10 N. Jayaprakash, J. Shen, S. S. Moganty, A. Corona and L. A. Archer, *Angew. Chem., Int. Ed.*, 2011, **50**, 5904.
11 G. He, X. Ji and L. Nazar, *Energy Environ. Sci.*, 2011, **4**, 2878.
12 X. Liang, Z. Wen, Y. Liu, H. Zhang, L. Huang and J. Jin, *J. Power Sources*, 2011, **196**, 3655.
13 B. Zhang, X. Qin, G. R. Li and X. P. Gao, *Energy Environ. Sci.*, 2010, **3**, 1531.
14 S. Li, M. Xie, J. B. Liu, H. Wang and H. Yan, *Electrochem. Solid-State Lett.*, 2011, **14**(7), A105.
15 X. Li, Y. Cao, W. Qi, L. V. Saraf, J. Xiao, Z. Nie, J. Mietek, J.-G. Zhang, B. Schwenzer and J. Liu, *J. Mater. Chem.*, 2012, **21**, 16603.
16 M. Nagao, A. Hayashi and M. Tatsumisago, *J. Mater. Chem.*, 2012, **22**, 10015.
17 L. Le Leuch, A. Subrenat and P. Le. Cloirec, *Langmuir*, 2003, **19**, 10869.
18 L. Truong and N. Abatzoglou, *Biomass Bioenergy*, 2005, **29**, 142.
19 M. Endo, T. Maeda, T. Takeda, Y. J. Kim, K. Koshiba, H. Hara and M. S. Dresselhausb, *J. Electrochem. Soc.*, 2001, **148**(8), A910.
20 D. Qu and H. Shi, *J. Power Sources*, 1998, **74**, 99.
21 Y.-G. Wang and Y.-Y. Xia, *J. Electrochem. Soc.*, 2006, **153**(2), A450.
22 F. Wu, S. X. Wu, R. J. Chen, S. Chen and G. Q. Wang, *Chin. Chem. Lett.*, 2009, **20**, 1255.
23 W. Yong-Gang and X. Yong-Yao, *J. Electrochem. Soc.*, 2006, **153**(2), A450.
24 H.-S. Ryu, H.-J. Ahn, K.-W. Kim, J.-H. Ahn and J.-Y. Lee, *J. Power Sources*, 2006, **153**, 360.
25 X. He, J. Ren, L. Wang, W. Pu, C. Jiang and C. Wan, *J. Power Sources*, 2009, **190**, 154.

 